Long-Range Predictability in the Tropics. Part I: Monthly Averages

THOMAS REICHLER* AND JOHN O. ROADS

Scripps Institution of Oceanography, University of California, San Diego, La Jolla, California

(Manuscript received 10 March 2003, in final form 24 June 2004)

ABSTRACT

The sensitivity to initial and boundary conditions of monthly mean tropical long-range forecasts (1–14 weeks) during Northern Hemisphere winter is studied with a numerical model. Five predictability experiments with different combinations of initial conditions and prescribed ocean boundary conditions are conducted in order to investigate the temporal and spatial characteristics of the perfect model forecast skill. It is shown that initial conditions dominate a tropical forecast during the first 3 weeks and that they influence a forecast for at least 8 weeks. The initial condition effect is strongest over the Eastern Hemisphere and during years when the El Niño–Southern Oscillation (ENSO) phenomenon is weak. The relatively long sensitivity to initial conditions is related to a complex combination of dynamic and thermodynamic effects, and to positive internal feedbacks of large-scale convective anomalies. At lead times of more than 3 weeks, boundary forcing is the main contributor to tropical predictability. This effect is particularly strong over the Western Hemisphere and during ENSO. Using persisted instead of observed sea surface temperatures leads to useful forecast results only over the Western Hemisphere and during ENSO.

1. Introduction

The skill of numerical weather prediction models in forecasting the Tropics at short to long ranges has always tended to lag that in the midlatitudes (Kanamitsu 1985; Reynolds et al. 1994). Forecasting tropical variations is not only complicated by the lack of good observations, but also by the relative complexity of tropical dynamics, which are governed by different balances than the extratropics. Outside the Tropics, quasigeostrophic theory provides a relatively simple theoretical framework for an overall understanding of large-scale motions. In the Tropics, however, this concept breaks down, since pressure gradients and the Coriolis parameter are too small for motions to be in geostrophic balance. Other effects like friction and diabatic and latent heating become important. The release of latent heat associated with precipitation from convective cloud systems represents the dominant source of energy in the Tropics. This process, however, is difficult to simulate, and therefore represents a great challenge for our models.

* Current affiliation: Department of Meteorology, University of Utah, Salt Lake City, Utah.

Corresponding author address: Dr. John O. Roads, Scripps Institution of Oceanography, University of California, San Diego, 9500 Gilman Dr., La Jolla, CA 92093-0224.
E-mail: jroads@ucsd.edu

The goal of this study is to characterize the spatial and temporal structure of the predictability in the Tropics and to find out how important the contributions of initial conditions (ICs) and boundary conditions (BCs) are for such predictability. On time scales of seasons or longer, the Tropics are certainly dominated by the forcing from the sea surface temperatures (SSTs) underneath (e.g., Shukla 1998). However, on subseasonal time scales, which are the focus of this study, the relative role of initial and boundary conditions is more complicated. Recently, Reichler and Roads (2003, hereafter referred to as RR) found that in the Tropics, initial conditions dominated a numerical forecast for several weeks. This relatively long time scale was surprising and prompted further analysis aimed at finding the reasons for this large sensitivity to initial conditions. As we will see, there appear to be two mechanisms by which initial conditions are important for the tropical forecasting problem: first, the intraseasonal or Madden–Julian oscillation (MJO; Madden and Julian 1994), and second, the slow response of the tropical atmosphere to changes in boundary conditions. Predictability issues related to the MJO are the subject of a companion paper (Reichler and Roads 2005). In it, we investigate tropical predictability at periodicities of 30–60 days and find that initial conditions are crucial for predicting the MJO, although important responses to external SST forcing do exist.

The present paper is focused on the atmospheric predictability of monthly averages at lead times from 15 days to one season. This time scale has not received much attention in previous studies of tropical predictability, which were focused almost exclusively on the predictability of the intraseasonal oscillation. The problem of predicting monthly averages is influenced by both interannual variability related to the El Niño–Southern Oscillation (ENSO) phenomenon, and by intraseasonal variability related to the MJO. However, since the MJO exhibits variability on a broad spectrum with periods between 30 and 90 days, much of the MJO variability is removed by taking monthly averages.

We used a model-based approach to answer our questions and conducted five idealized ensemble experiments with a complex atmospheric general circulation model (AGCM). Each experiment was forced with different combinations of initial and boundary conditions to determine individual and cumulative contributions of each to the inherent predictability. Ensemble forecasts were performed over many years to separate unpredictable noisy components from the various signals. We analyzed predictability of four representative atmospheric variables by measuring their so-called "perfect model forecast skill." Under this approach, model output is verified against the output of a control experiment using the same model (Buizza 1997; Anderson et al. 1999). This eliminated complications with model-dependent errors and allowed us to focus exclusively on the key questions of this study. Another idealization of this study is the use of prescribed ocean boundary conditions, which assumes that the future evolution of the ocean is perfectly known at the time of the forecasts. In real forecast situations, however, SSTs are not known a priori. The generality of our results depends also on the proper response of the model to boundary forcing and in particular on the ratio of the forced to the unforced variability. Therefore, this study investigates a potentially hypothetical upper limit of perfect model predictability, which is derived from specific variables of a specific model. In this study, we call this simply "predictability." Practical predictability is likely to be lower than our predictability measure, since observational data would be needed to verify an imperfect model and since predicted ocean data would be needed to force an imperfect model.

In section 2, we briefly describe the model, experiments, and analysis techniques used for this study. In section 3, we present a short discussion of the model's climatology in comparison with observational data. Section 4 discusses the temporally and spatially varying character of tropical predictability using different initial and boundary conditions. Section 5 investigates further aspects of the long initial condition memory. Summary and conclusions are provided in section 6.

2. Methodology

a. Model and experiments

The AGCM of this study was the National Centers for Environmental Predictions (NCEP) seasonal forecasting model (e.g., RR; Kanamitsu et al. 2002b). We used the model at T42 resolution with 28 vertical levels to conduct five ensemble experiments. Each experiment consisted of many 107-days-long continuous simulations of the Northern Hemispheric winter season from 15 December to the end of the following March. The experiments were carried out in an ensemble mode, with an ensemble size of 20 for the control simulation "ICBC" and 10 for the other experiments. A total of 22 winter seasons (1979–2000) were simulated, so that each experiment consisted of a total of 220 (440) continuous runs.

The members of one experiment and year were forced with identical boundary conditions but were started from slightly perturbed initial conditions. To create those initial conditions, two continuous Atmospheric Model Intercomparison Project (AMIP)-type base runs with either observed (BASE-O) or climatological (BASE-C) ocean boundary conditions were carried out. For each year, the appropriate initial conditions for the subsequent experiments were derived from those base runs and perturbed by using the breeding method (Toth and Kalnay 1997). The resulting mean rms error between individual perturbed initial conditions at the 850- (200) hPa level over the Tropics was $\sim$3 (6) m s^{-1} for the u and v wind components, and $\sim$14 (25) m for the geopotential height. The interested reader is referred to RR for more specific information about the implementation of the breeding method.

The five ensemble experiments of this study differed only in the specification of their initial and boundary conditions (see Table 1). The experiments were global, and initial and boundary conditions were modified globally. However, in the analysis presented here, only the local response in the Tropics was examined. We identify the five experiments by specific acronyms, which indicate the quality of ICs and BCs used.

Experiment ICBC was forced with observed ocean boundary conditions and was started from "anomalous" initial conditions of BASE-O. Under the perfect model approach, all experiments are verified against ICBC. ICBC verified against itself is therefore similar to a classical predictability experiment where the divergence of solutions starting from slightly different initial states is measured. The only difference is that ICBC uses anomalous boundary forcing, which helps to support the anomalous initial state. Experiment "IC" used the same perfect initial conditions as ICBC, but was forced with climatological ocean and land boundary conditions. This experiment was designed to measure the effect of anomalous initial conditions, which are created by, but which are not supported by, boundary forcing. Experiment "BC" represents the complementary experiment to IC and was designed to study the effects of boundary forcing alone. It was started from randomly chosen "climatological" initial conditions from BASE-C but was forced with the same perfect boundary conditions as ICBC. Experiment "ICP" was

Table 1. Boundary and initial conditions, ensemble size, and simulation period for each experiment of this study. Winter refers to 15 Dec–31 Mar of the following year, "rndm" indicates randomly chosen initial conditions, "clim" indicates climatological boundary conditions, "cont" indicates continuous base run over all years, "obs" means observed (i.e., reanalysis-1), and "R-2" indicates NCEP–DOE reanalysis-2.

Name	Boundary conditions: Ocean	Boundary conditions: Land	Initial conditions: Atmosphere	Initial conditions: Land	Size	Period	Years
BASE-O	Obs	Model	Obs 1/1/48	Obs 1/1/48	1	Cont	1948–2000
BASE-C	Clim	Model	Obs 1/1/48	Obs 1/1/48	1	Cont	1948–2024
ICBC	Obs	Model	BASE-O	BASE-O	20	Winter	1979–2000
ICP	Persisted	Model	BASE-O	BASE-O	10	Winter	1979–2000
IC	Clim	R-2 clim	BASE-O	—	10	Winter	1979–2000
BC	Obs	Model	BASE-C rndm	BASE-C rndm	10	Winter	1979–2000
iBC	Obs	Model	ICBC, 1-yr lag	ICBC, 1-yr lag	10	Winter	1980–2001

again started from the same initial conditions as ICBC but used persisted ocean boundary conditions. Persisted SSTs means that the SST anomaly at day 0 of a specific seasonal simulation is simply persisted around the seasonal cycle during the whole integration. This is a common alternative to more sophisticated ocean forecast techniques (e.g., Mason et al. 1999; Roads et al. 2001), since at time scale of up to 3 months it is usually more accurate than other forecast methods (e.g., Goddard and Mason 2002). Finally, experiment "iBC" was started from initial conditions by integrating ICBC for one whole year. These initial conditions have completely lost their memory from the previous year, but they are adjusted to the boundary forcing at the new initialization time. In this respect, experiment iBC was comparable to an ensemble of continuous AMIP-type integrations, and to the current operational seasonal forecasting methodology at the International Research Institute (IRI). The motivation for iBC was to find out how much predictability might be lost by excluding the effects of perfect synoptic scales in the initial conditions.

b. Data

The ocean boundary conditions for the five experiments of this study were prescribed using observational data. The SSTs came from the Met Office Global Ice and Sea Surface Temperature (GISST) dataset for the 1950–81 period, and afterward, from Reynolds SSTs (Reynolds and Smith 1994) with a weekly temporal resolution. The sea ice data were taken from daily NCEP–NCAR reanalysis (Kalnay et al. 1996; Kistler et al. 2001). Climatological ocean boundary conditions were derived by averaging the observed fields over the 50-yr period of 1950–99. The land boundary conditions were either determined internally by the land surface model of the AGCM or prescribed from the NCEP–Department of Energy (DOE) AMIP-II reanalysis (R-2; Kanamitsu et al. 2002a) by averaging from 1979 to 1998. For the verification of the model climatologies, either NCEP–NCAR reanalysis or Climate Prediction Center Merged Analysis of Precipitation (CMAP) data (Xie and Arkin 1997) were used.

c. Calculation of forecast skill

We estimated the atmospheric predictability from the forecast skill of four representative variables: the velocity potential at 200 hPa (χ200), the zonal wind at 850 hPa (U850), the temperature at 850 hPa (T850), and the precipitation rate. Before the forecast skill was calculated from the simulation time series, anomalies were computed by removing the daily climatology of the corresponding simulation. Next, the time series were filtered in time by taking 31-day running averages. This procedure has a low-pass characteristic with a cutoff period of about 60 days. It therefore retained interannual variability that is mostly related to ENSO, and intraseasonal variability at periodicities of 60 days and more, which is largely related to the tropical intraseasonal oscillation. Since filtering of the beginning and end of the seasonal time series would have required additional data, the first and last 15 days were excluded from our calculations.

The forecast skill between an experiment and the control run ICBC was estimated in two ways. First, the temporal correlation (TC) of the year-to-year time series for a certain lead time was used to construct maps of forecast skill. Second, the spatial anomaly correlation (AC) over the Tropics was calculated from data for the same lead time and year, and then averages were taken over the various years. Throughout this study, the Tropics were defined as the region from 30°N to 30°S latitude and from 0° to 360° longitude. To mimic real forecast situations, the correlations were calculated between the 10-member ensemble mean of the individual experiment under consideration and individual realizations of the control experiment ICBC. Since 20 members of ICBC were available as verification, a more robust skill estimate was obtained by selecting each member of ICBC as verification and by averaging over the individual outcomes. The verification of ICBC with itself gave the upper bound of perfect model predictability, since in this case boundary conditions were perfect, and initial conditions were almost perfect. Only the small perturbations in the initial conditions led to a divergence of the solutions for the various ensemble members, which thus contributes to a decrease in predictability over time. The appendix explains in more detail the treatment of the data and the calculation of the forecast skill.

The forecast base period was 1979–2000, but in some of our analysis, the forecast skill was calculated only over a subset of years. For example, strong ENSO warm years were the winters of 1983, 1987, 1992, and 1998, and strong cold years were 1985, 1989, 1999, and 2000. Neutral to weak ENSO years were all of the other 14 yr from the 1979–2000 period.

3. Observed and simulated tropical climate

To find out how realistic the simulations of the AGCM were, we describe in this section the climatology and the interannual variability of the four variables from the perfect experiment ICBC and compare them with observational data. The analysis is focused on January monthly means and covers the 22-yr period from 1979 to 2000. For simulation ICBC, the climatology was derived from the average of all 20 ensemble members, and the interannual variability was calculated for individual members and then averaged together.

In Fig. 1, the observed January climatologies are compared with that from simulation ICBC. In general, the structure and amplitude of all four simulated variables compared reasonably well with observations, in particular for U850 and T850 (Fig. 1, middle). Differences between model and reanalysis were most noticeable for $\chi 200$ (Fig. 1, top). While the model simulated three distinct centers of convective activity over the Indian Ocean, the warm pool region, and South America, the reanalysis did not show as clear a separation into three different regions. Moreover, the divergent circulation in the model was too strong over the date line and too weak over the Indian Ocean. Besides model deficiencies, these discrepancies may be in part attributable to the fact that the divergent circulation is not really an observed quantity. It largely depends on the convective parameterization scheme of the model used, and the schemes are different in the reanalysis model and the model of this study. Figure 1 (bottom) compares the amount of simulated and observed tropical precipitation. This quantity is also strongly related to convective activity. In this case, the observations were derived from satellite and rain gauge data (CMAP) and did not contain any model biases. The largest model deficits existed over South America with too much rainfall and over the Indian Ocean and Maritime Continent with too little rainfall. Over the Indian Ocean, the model exhibited a double intertropical convergence zone structure, a problem which is typical for many AGCMs. Note, however, that the precipitation rate near the date line was about right and that the characteristic South Pacific convergence zone was simulated quite well.

Figure 2 compares the interannual variability between observations (left) and simulation ICBC (right).

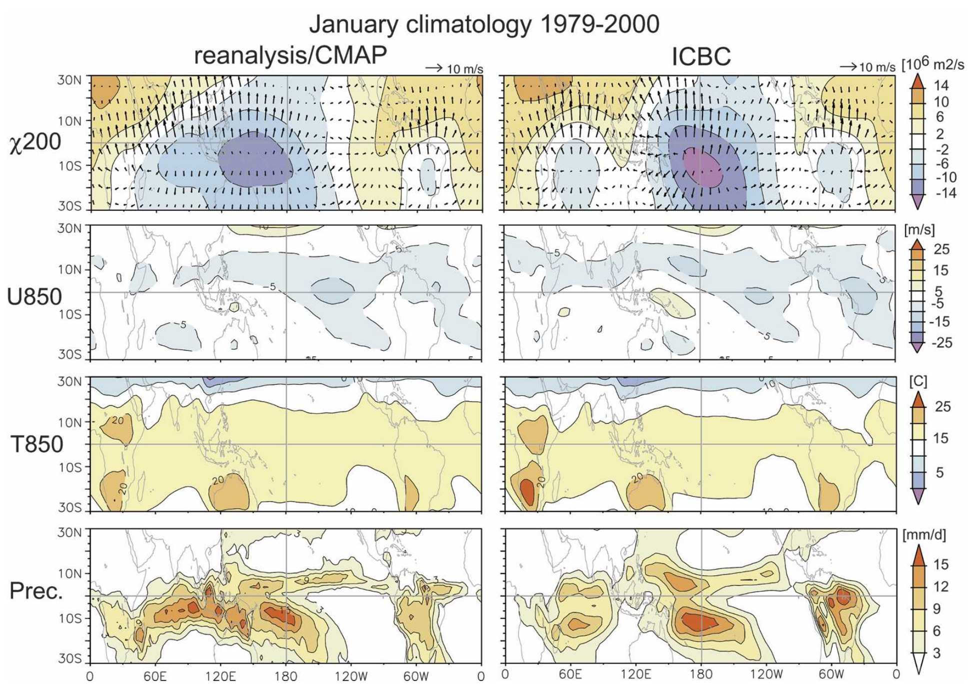

FIG. 1. The Jan monthly mean climatology (1979–2000) of velocity potential (in 10^6 m^2 s^{-1}) and divergent winds (arrows) at 200 hPa, zonal winds (in m s^{-1}) at 850 hPa, temperature (in °C) at 850 hPa, and precipitation (in mm day^{-1}): (left) the NCEP–NCAR reanalysis (CMAP for precipitation) and (right) simulation ICBC.

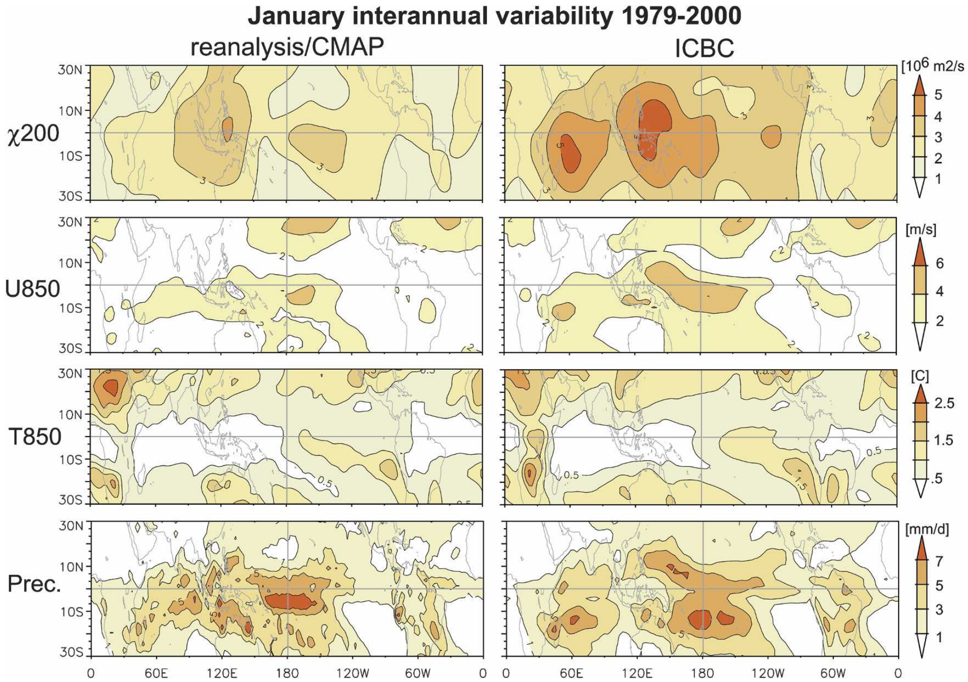

FIG. 2. The Jan monthly mean interannual standard deviation of the four selected variables. See Fig. 1 for more details.

In general, the model showed a larger interannual variability than the observational data, in particular for $\chi 200$ (Fig. 2, top). For this quantity, the simulated variability was much larger than in reanalysis, especially over the Indian Ocean and the warm pool region. Again, it may well be that the reanalysis underestimated the $\chi 200$ variability, since the AGCM of this study presumably uses a physically more realistic convection scheme [relaxed Arakawa–Schubert (RAS)] than the reanalysis [simplified Arakawa–Schubert (SAS)]. This explanation is supported by the fact that the differences between simulated and observed rainfall variability (Fig. 2, bottom) from CMAP data are much smaller than for $\chi 200$.

We were also interested to find out how much intraseasonal variability remained in the data after taking monthly means. We depict in Fig. 3 the ratio between the interannual and the intraseasonal variance (VIA/VIS of $\chi 200$ for both the reanalysis and experiment ICBC. The intraseasonal variability is smaller by about a factor of 2–4 than the interannual variability. As expected, the ratio is largest over the equatorial Pacific. Again, the large-scale structures for reanalysis and model data are very similar.

In summary, the model did not reproduce exactly every aspect of the observed atmosphere, but it captured the basic patterns quite well. Therefore, we are confident that this AGCM is an adequate tool for the investigation of tropical low-frequency predictability.

4. Analysis of forecast skill

In the following section we examine the tropical long-range forecast skill of monthly means from our five model experiments. First, we show geographical maps of temporal correlation at a fixed lead time interval of 1 month, next we examine the spatial anomaly

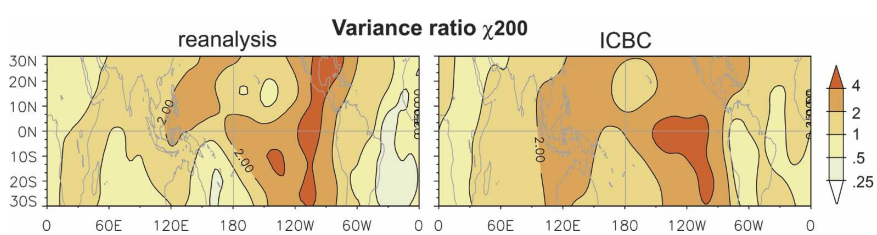

FIG. 3. The ratio between the interannual (VIA) and the intraseasonal variance (VIS) of 200-hPa velocity potential for (left) the reanalysis and (right) experiment ICBC.

correlation over the tropical domain in its entire temporal evolution, and finally we analyze the interannual variations in forecast skill.

a. Spatial structure

Figure 4 shows the spatial structure of monthly mean forecast skill over the Tropics during January as measured by the temporal correlations over all 22 yr. Since the experiments were initialized on 15 December, the January mean correlations correspond to roughly a 1 month lead time, or in other words to forecasts of week 3–6.

The correlations for ICBC (Fig. 4, top) give an estimate for the upper bound of predictability at this lead time and with this model, since both initial and boundary conditions were perfect. The correlations for $\chi200$ (first column) are more evenly distributed than that of the other fields, since velocity potential is a very smoothly varying quantity. All four variables exhibit maximum correlations in a relatively narrow band over the Pacific cold tongue region, coinciding well with the region of maximum ENSO related interannual SST variability (not shown). In general, the correlations over the Eastern Hemisphere (0°–180°E) are lower than over the Western Hemisphere (0°–180°W). The low-level temperatures show a large region with very high correlations over the equatorial Pacific, presumably due to the direct thermal effect of SST forcing on this quantity.

The correlations for experiments BC and iBC are presented in the next two rows. These two experiments were forced with perfect boundary conditions but were started from imperfect initial conditions. The difference of their correlations to ICBC measures how much forecast skill can be attributed to boundary forcing alone and how much skill is lost by not having good initial conditions. At first sight, the correlations are very similar to ICBC, indicating that the effects of boundary forcing on monthly averaged forecast skill are overwhelming at this lead time interval. A more careful examination reveals that the correlations for each variable are almost everywhere smaller than ICBC and that the effects of poor initial conditions are noticeable. This is also indicated by the area-averaged correlations in the top left corners. Experiment BC has on average a somewhat larger loss in skill than iBC, indicating that the adjusted initial conditions of iBC are a better choice than the climatological initial conditions of BC. It also turns out that this loss in skill due to poor initial conditions is most noticeable over regions, which are away from the cold tongue region.

Experiment IC (fourth row), which was started from perfect initial conditions but was forced with climato-

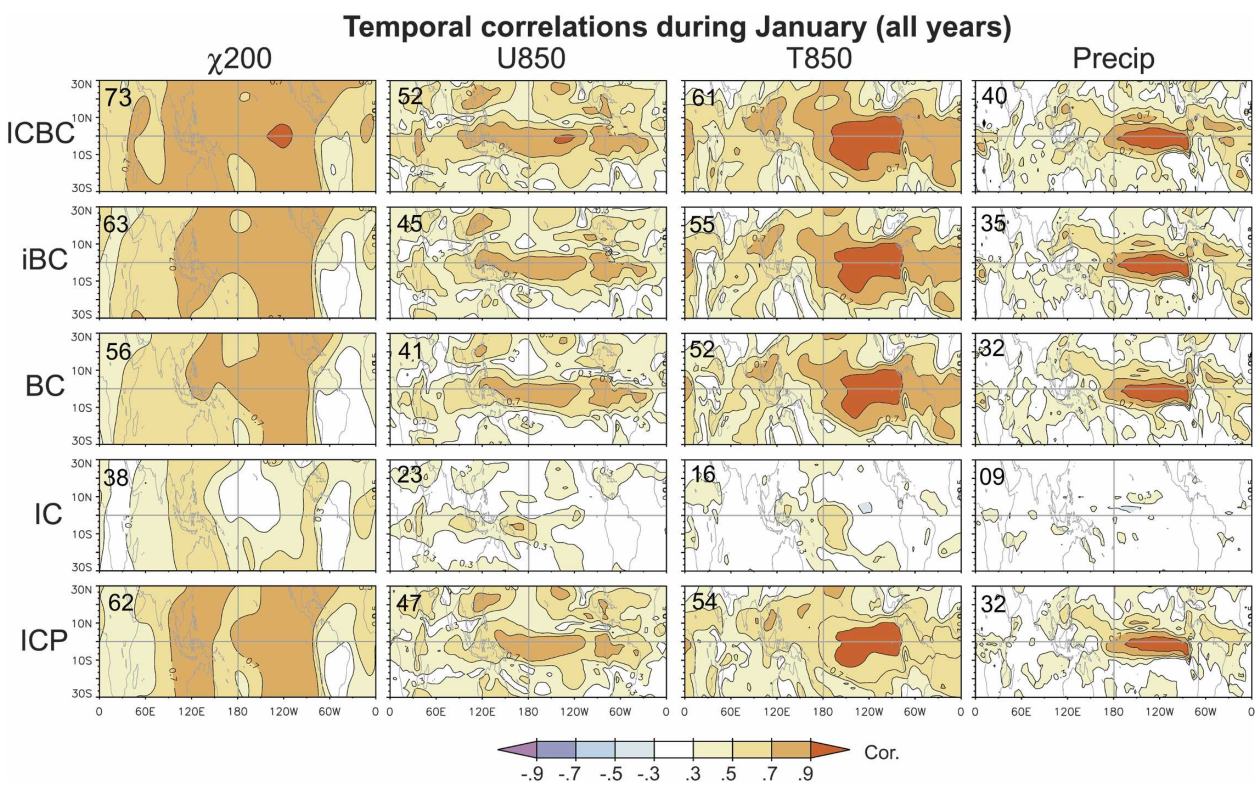

FIG. 4. The temporal correlations (1979–2000) of Jan monthly mean model output, corresponding to the forecast skill of weeks 3–6. All experiments were verified against the perfect experiment ICBC. See Table 1 for definitions of ICBC, iBC, BC, IC, and ICP. The numbers in the top left corner of each panel indicate the area-averaged correlation.

logical boundary conditions, represents the complementary experiment to BC. The correlations for IC give a good measure of how much long-range predictability can be attributed to the effect of initial conditions alone and how long time it takes for the wrong boundary forcing to overcome the initial condition effects. It is not surprising that the correlations for IC are much lower than for ICBC, in particular over the equatorial Pacific. It is interesting, however, that initial conditions alone produce small but nontrivial forecast skill over many regions and for all variables. This is particularly evident for the upper-level velocity potential, but even precipitation has small regions of predominately positive correlations. The correlations for IC are usually larger over the warm pool region and over the Indian Ocean, areas where experiment BC had the largest loss in forecast skill. Conversely, this is true too. This suggests that to first order the different predictability effects of initial and boundary conditions are linear and that they can be simply added up to the full predictability field of ICBC.

The patterns of predictability for experiment ICP, which was forced with persisted SSTs and was started from the same initial conditions as ICBC, are shown in the bottom row. Even though the correlations are similar to ICBC, one can notice a spatially quite uniform decrease in correlations, which can be ascribed to the effect of having lower-quality boundary conditions.

The above results confirm earlier studies in that boundary forcing is the main contributor to forecast skill in the Tropics. However, we also found that initial conditions have a small but nevertheless measurable effect on tropical predictability at a lead time of 1 month. The fact that experiments with good boundary conditions exhibited largest correlations over the cold tongue region and the fact that the initial condition effect was most noticeable away from this region suggests that the boundary-forced predictability was mostly related to interannual SST variations due to ENSO. It is likely that the more subtle initial condition effect was offset over this region by the dominating boundary effect.

To investigate this assumption further, we repeated the above calculation but included only years from neutral to weak ENSO years in the calculation of the temporal anomaly correlations (Fig. 5). In this case, boundary effects from ENSO-related SST variability were much weaker, so that the correlations were smaller. This reduction in skill was most noticeable over the cold tongue region, whereas other areas were far less affected. As expected, by selecting only neutral to weak ENSO years, the relative effect of initial conditions became more important. This can most clearly be seen over the warm pool region, where experiment IC had higher correlations than experiments iBC or BC. The results for experiment ICP indicate that persisting SSTs

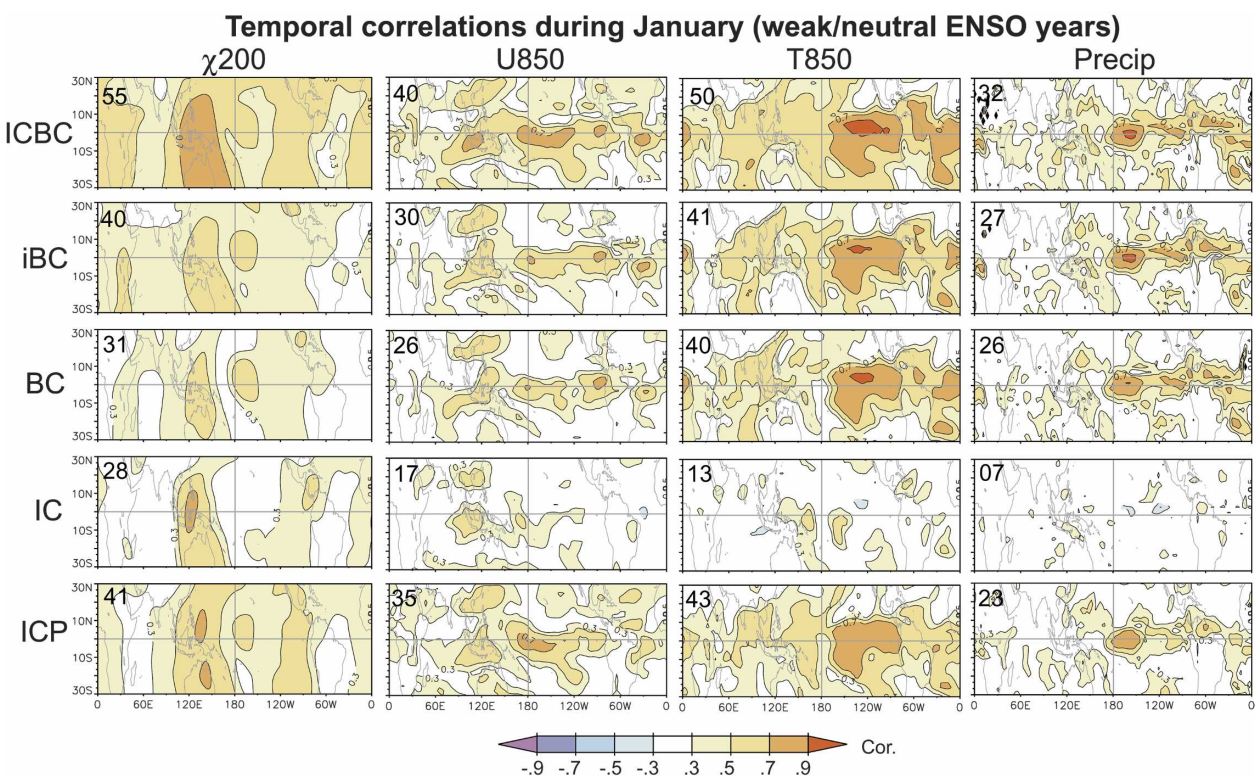

FIG. 5. Same as in Fig. 4, but for weak to neutral ENSO years only.

during years with weak ENSO forcing leads to a stronger loss in forecast skill than when including all years.

b. Lead time evolution

Next, we investigate the spatial AC over the entire tropical domain as a continuous function of lead time. Figure 6 shows the evolution of the ACs in daily increments from day 16 (30 December) out to day 92 (16 March) for the five experiments and four variables. The left side of Fig. 6 depicts ACs averaged over all 22 yr (1979–2000), and the right side shows average ACs for neutral to weak ENSO years. The ACs were calculated for each time step, ensemble member, and year, and the results from different years and members were averaged using the Fisher z-transformation. The thin continuous lines in Fig. 6 depict the skill of a persistence forecast, which is made simply by persisting day 0 of ICBC for all lead times. Note that the correlations at lead times of 32 days correspond to January monthly means, which were discussed in the previous section for the temporal correlations.

First, we discuss what one would expect theoretically for the different cases. Experiments with "perfect" initial conditions (ICBC, IC, and ICP) should start with correlations of close to one. The initial correlations are not expected to be exactly one since 1) the initial conditions were perturbed, and 2) monthly averages were taken. Then, as the solutions for the individual ensemble members diverge, the correlations should decrease at a rate that depends on the quality of the boundary conditions. The decrease for IC should be fastest since the anomalous initial conditions are unsupported by the boundary forcing. The correlation for ICBC, on the other hand, should be largest since the boundary conditions are perfect. At longer lead times, the correlations for ICBC should reach some asymptotic value that depends on the strength of the effects of boundary forcing on forecast skill. The correlations for ICP should decrease at some intermediate rate as the error from using persisted boundary conditions increases in time. For experiment BC, one would expect zero skill at the beginning since it starts from wrong initial conditions. Then, the correlations for BC should increase and approach the same asymptotic value as ICBC. Finally, experiment iBC should show a constant skill in time equal to the asymptotic value of ICBC, since in this case the atmosphere is at all times adjusted to the boundary forcing. One may expect some temporal variations in this asymptotic value as the strength of the boundary forced signal undergoes seasonal variations. In this context, the seasonal variations of the ENSO signal, which typically peaks during early winter, are important.

Figure 6 shows that the measured correlations for the predictability experiments follow the expected behavior quite well. The four variables show different levels of basic skill, which is linked to the spatial and temporal variability of their fields. The correlations from experiment ICBC reflect the maximum potential predictability with this model. At short lead times, the skill is high because of the initial condition effect. After several weeks, when the initial condition effect is presumably close to zero, and when mostly boundary forcing affects predictability, the correlations reach their asymptotic value. The size of this value depends on the type of variable and over which years the ACs were averaged. During all years, χ200 levels out at correlations of about 0.7, followed by U850 at 0.5 and by precipitation and T850 at 0.4. Even during neutral to weak ENSO years, this boundary condition–produced perfect model forecast skill is rather high: 0.5 correlation for χ200, 0.4 for U850, and about 0.3 for T850 and precipitation. This indicates that even weak ENSO events and non-ENSO-related SST forcing lead to a rather high signal-to-noise ratio for the tropical atmosphere. For the interpretation of this result, one has to bear in mind that the sensitivity of the model to external forcings may differ somewhat from the response by the real atmosphere.

The correlations for iBC are generally higher than that for BC, which is consistent with the different qualities of their initial conditions. We recall that iBC comes from fully adjusted initial conditions, and BC comes from climatological initial conditions. The differences to ICBC measure how much forecast skill is lost from excluding the initial condition effect. Averaged over all variables and time periods, it took about 50 days for simulation iBC to approach the same level of skill as ICBC. Experiment BC basically never reached the skill of ICBC, not even at the longest lead times.

The correlations for experiment IC demonstrate how much skill is lost when the boundary forcing does not support anomalous initial conditions. There is a rapid decrease in correlations during the first 30 days and a slow asymptotic descent to zero skill thereafter. Zero skill is reached at 60 days or later. An objective measure for the relative importance of initial and boundary conditions is given by the time when the curves from IC and BC intersect. This time scale indicates how long initial conditions dominate the forecast result. It is on the order of 3 weeks for these experiments and variables.

The correlations for the simple atmospheric persistence forecasts are indicated by the thin continuous curves in Fig. 6. During the first 40–60 days, they were smaller than the correlations of experiment IC, indicating that not only simple atmospheric persistence is responsible for the initial condition effect. This demonstrates the beneficial effects of a dynamical model on forecast skill. It is not surprising that at longer lead times the atmospheric persistence forecast had better skill than experiment IC, but the overall correlations were very small.

The temporal evolution of the skill for experiment ICP is shown by the dashed–dotted curves. The added uncertainty introduced by persisted SST anomalies translates in all four variables to significant losses in

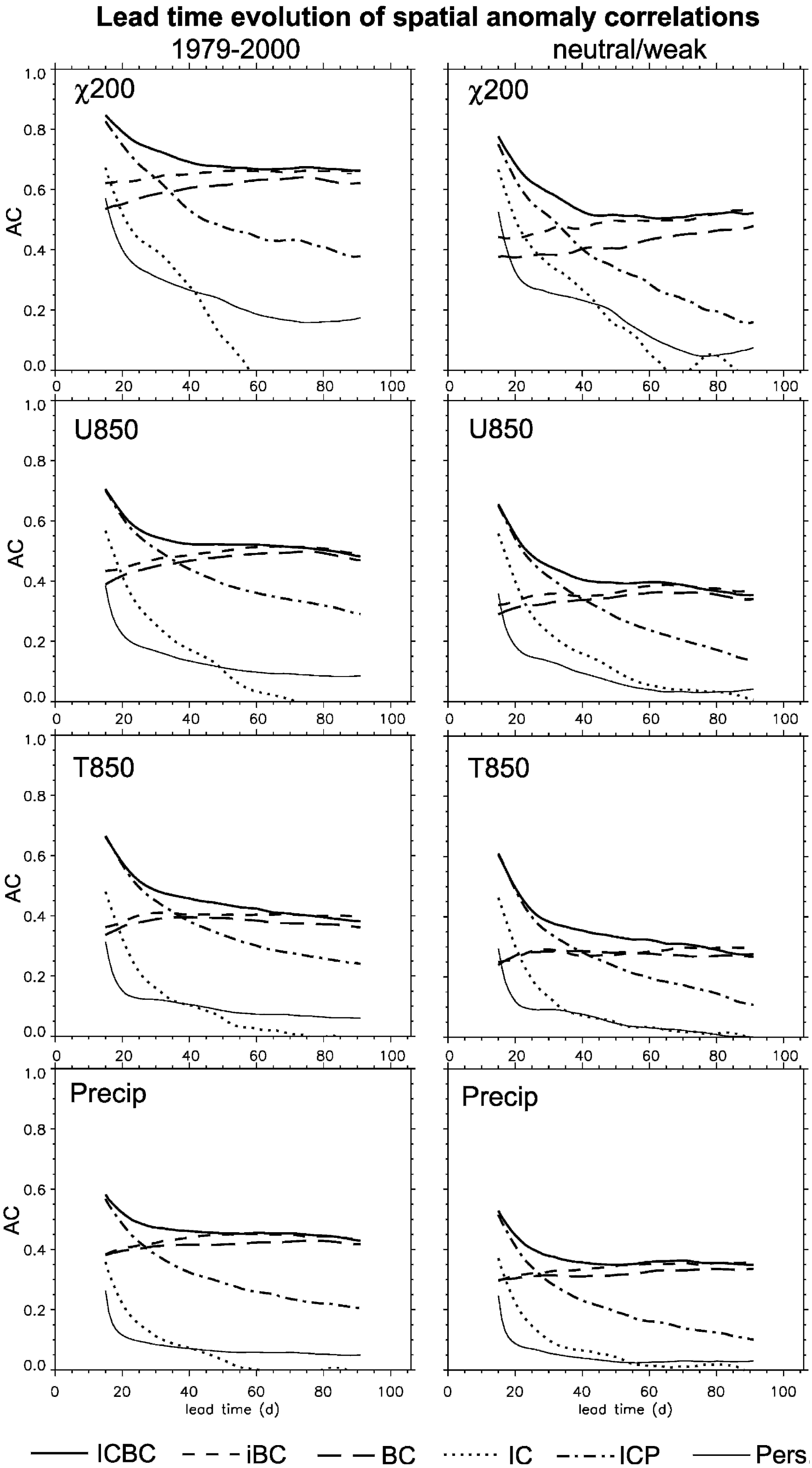

FIG. 6. The lead time evolution of the spatial anomaly correlation from low-pass-filtered model output for the five experiments of this study and for four different variables: (left) average ACs over all years and (right) averages over neutral to weak ENSO years. The vertical axis denotes AC.

skill as compared to the skill of experiment ICBC given perfect SST forcing. Thus, even though the ocean has a much longer time scale than the atmosphere, the assumption that current SSTs will be an accurate forecast of future oceanic conditions does not hold for the purpose of long-range atmospheric predictions. As will be discussed in the next section, there exist certain exceptions to this conclusion, since the persistent structure of SSTs is in general a function of season, year, and region.

In Fig. 7, we present a year-to-year breakdown of the spatial ACs of χ200 over the tropical domain for January monthly means. This time period corresponds roughly to forecasts of week 3–6. The years are arranged according to the correlations for experiment ICBC (black bars). The rather large correlations of experiments ICBC, iBC, and BC during ENSO years demonstrate how important interannual SST variations were during those years for the good overall skill. It is interesting to note that the correlations for IC were surprisingly large during some years—including years when ENSO was in its cold period (e.g., 1989 and 1999).

5. Characteristics of the initial condition effect

In the previous section, we found that initial conditions dominated tropical forecasts during the first 3 weeks and that even thereafter, initial conditions still affected the forecast. This seemed to be particularly strong over the Indian Ocean and during cold ENSO years. In the following, we further investigate the effects of initial conditions on tropical forecasts.

Figure 8 shows composites of height–longitude cross sections of the anomalous divergent circulation during January. The composites were taken over the four cold ENSO years. The plots represent meridional averages from 0° to 20°S to capture the center of convective activity during this time of the year. The patterns of experiment ICBC (top) show the typical response to ENSO cold events, with strong anomalous downward motion over the date line and compensating motions over most other areas. The patterns for IC (bottom) show that the atmosphere over the Western Hemisphere was, as expected, close to climatology, but over the Eastern Hemisphere, the patterns still resembled that of ICBC. This indicates that the atmosphere over the east was more persistent than over the west. We also investigated January composites from warm ENSO years (not shown). Curiously, a similar delayed response over the east to the now cooler-than-normal SSTs could not be found. Instead, the circulation of simulation IC during warm ENSO years was close to climatology almost everywhere.

The asymmetric behavior of the initial condition effect between the Eastern and Western hemisphere, and between cold and warm ENSO years, is further documented in Fig. 9. Shown here are the spatial anomaly correlations of low-pass-filtered forecasts for the two hemispheres and for the different phases of ENSO. The correlations for experiment IC (dotted line) show that the initial condition effect was stronger over the east than over the west and that it was stronger during cold than during warm ENSO years. During neutral to weak ENSO years, initial conditions seemed to be more equally important for the two hemispheres. During ENSO years, the correlations for the persistence forecast (thin continuous line) are generally higher over the west than over the east. The correlations for experiment ICP exhibit another interesting east–west asymmetry. During strong ENSO years, the loss in predictability from using persisted SSTs was quite small over the west, but it was large over the east. This may be related to the fact that ENSO-related SST anomalies over the equatorial Pacific are usually well developed during December and persist throughout the winter. However, the evolution of similar anomalies over the Indian Ocean lags that over the Pacific by about 1 month, so that persisting of SST anomalies from December leads to larger errors over the Indian Ocean in the following months.

6. Summary and discussion

We examined the sensitivity of monthly mean tropical forecasts to initial and boundary conditions during

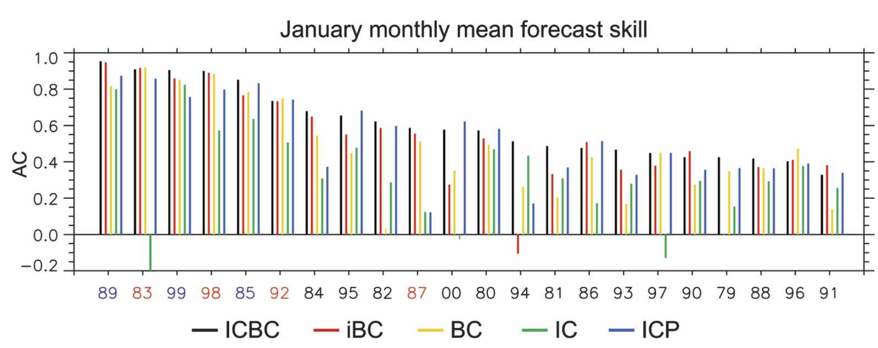

FIG. 7. The interannual variations of the spatial anomaly correlations at day 32, corresponding to Jan monthly means or weeks 3–6 forecasts. The years of cold (warm) ENSO years are shown by blue (red) numbers. Vertical axis denotes AC.

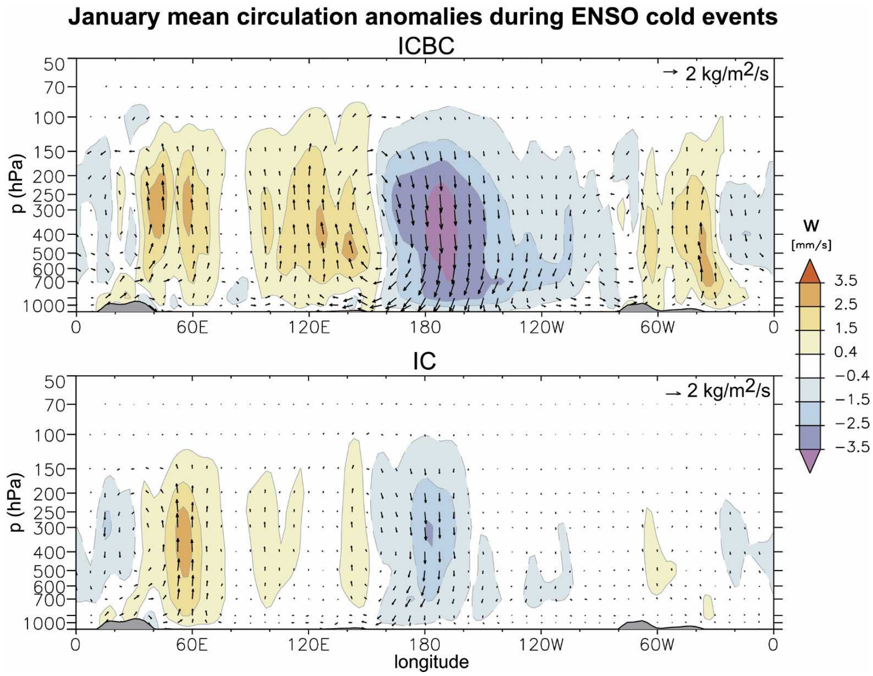

Fig. 8. Height–longitude cross section of Jan mean anomalous circulation during ENSO cold events, averaged from 0° to 20°S along the equator. Shown are the vertical velocity (shading, in mm s^{-1}) and the mass flux (vectors) from simulations (top) ICBC and (bottom) IC.

the boreal winter season at lead times from 1 to 14 weeks. We used a complex numerical model to conduct five predictability experiments with different combinations of initial and boundary conditions. When the model was forced with observed boundary conditions, the climatological mean and the interannual variability of the model atmosphere compared well with observational data. For each experiment, we examined the forecast skill of four representative variables, which were verified against the output of a control experiment with the same model.

Initial conditions dominated a tropical forecast during the first 3 weeks, and their influence lasted for at least 8 weeks. The initial condition effect was noticeable over all regions and during all years. It was strongest over the Indian Ocean and the warm pool region and during years with weak ENSO forcing. All four variables showed similar sensitivities. Boundary forcing was the main contributor to forecast skill at lead times of more than 3 weeks. Over the Tropics, the average anomaly correlation from boundary forcing alone was about 0.7 for upper-level velocity potential, 0.5 for lower-level winds, and 0.4 for lower-level temperatures and precipitation. When only weak to neutral ENSO years were included, the correlations were about 20% lower. The best forecast skill existed over the Pacific cold tongue region, which indicated the dominating effect of ENSO-related interannual SST variability on atmospheric predictability. Using persisted instead of observed SST boundary conditions started to have negative effects on the forecast skill after 2–3 weeks and led to considerable losses at longer lead times. All regions were affected, but the most sensitive regions were the Indian and the Atlantic Oceans. Persisted SSTs led to minor losses in skill only over the Pacific Ocean and during strong ENSO years.

A question remains as to what controls the initial condition memory of the tropical atmosphere and what sets the time scale of the response to boundary forcing. In general, the adjustment to boundary forcing is determined by a combination of dynamic as well as thermodynamic factors. Jin and Hoskins (1995) studied in detail the transient dynamic response to equatorial heating with a simple dry atmospheric model. They found the following chain of events after a specified equatorial heating was turned on: First, the heating rapidly induced local equatorial ascent and upper-tropospheric divergence. Then, to the east of the heating-region fast-propagating Kelvin waves appeared, and to the west and over the heating region, a slower Rossby wave response developed. The waves emanated from the heating region, and within 1 week an equivalent barotropic Rossby wave train propagated from the heating region into and through the winter hemisphere middle latitudes. Within the second week, wavenumbers greater than 4 were refracted back into the Tropics, where the waves finally interacted with the tropical atmosphere. From this dynamical perspective, one can

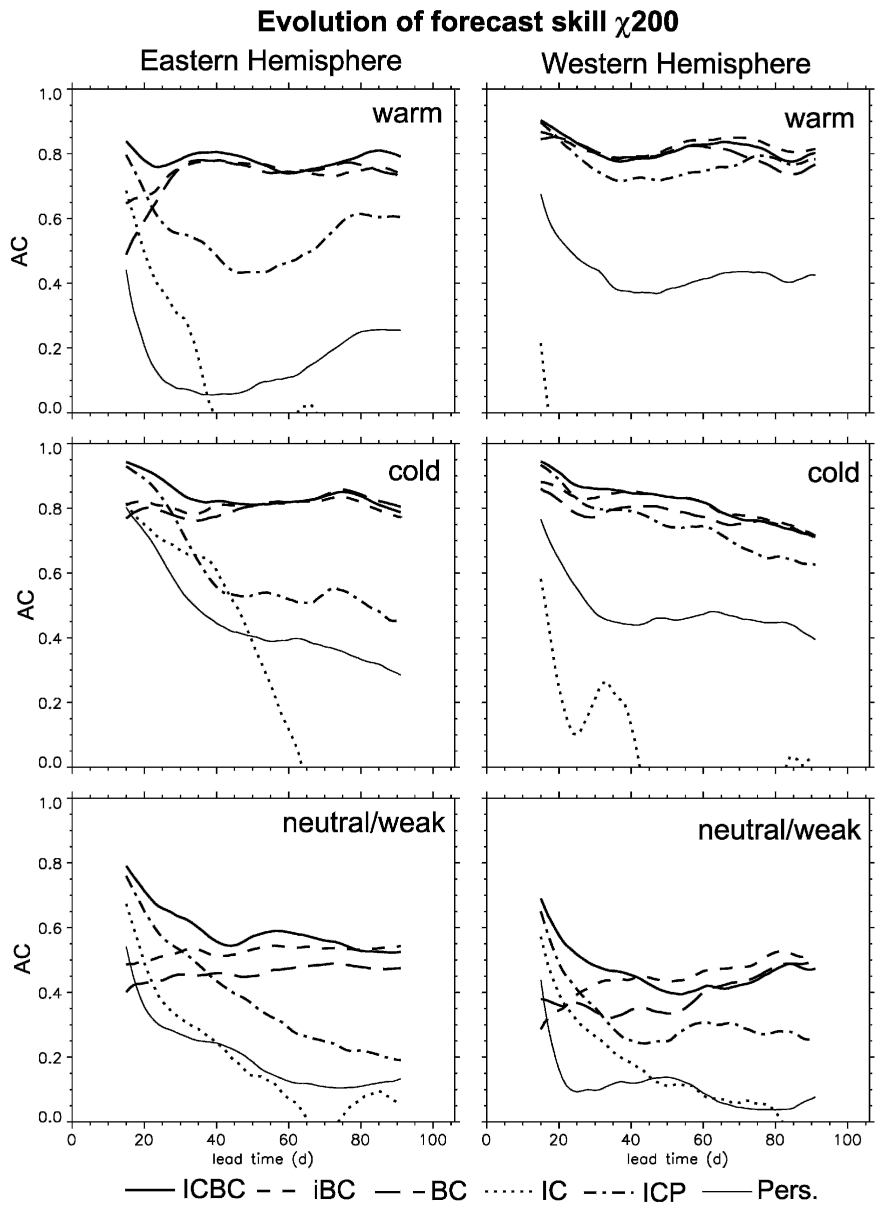

FIG. 9. Spatial anomaly correlation of low-pass-filtered 200-hPa velocity potential, calculated separately for the (left) Eastern (0°–180°) and (right) Western (180°–360°) Hemispheres and for (top) warm, (middle) cold, and (bottom) neutral to weak ENSO years. See Table 1 for definitions of ICBC, iBC, BC, IC, and ICP.

estimate that the tropical atmosphere adjusts to anomalous diabatic heating within three weeks or so. This time scale is in rather good agreement with the results of our experiments.

The time scale of the initial condition effect in the Tropics can be explained, in part, by thermodynamic arguments. It is well known that the ENSO signature in the tropical tropospheric mean temperature data is lagged by about one to two seasons relative to the SSTs over the Pacific cold tongue (e.g., Newell and Wu 1992). Yulaeva and Wallace (1994) showed that this long adjustment time scale can be understood from a passive radiative and thermodynamic response of the coupled atmosphere–ocean system to SST forcing over the equatorial eastern Pacific. The long time scale is mainly due to the large heat capacity of the system, which is composed of the heat capacities of the atmosphere plus that of the topmost 10 m of the ocean. Our experiments were forced with prescribed SSTs, so that the effective heat capacity is solely determined by the atmosphere. This helps to explain why the adjustment time in our case is shorter than a season.

The initial condition effect may also be related to a balanced mixture of thermodynamic and dynamic effects if, for example, MJO phenomenon have an important influence. By taking monthly averages, however, most of the MJO-related variability was suppressed in the present study, so that those effects were likely to be less important. This became evident from the relatively small amount of intraseasonal variability. Again, we found that the divergent circulation over the Eastern Hemisphere was very persistent. This may be related to an inherent positive feedback of tropical convection, in the sense that preexisting convection can create favorable conditions for further convection. Over the Western Hemisphere, this persistent behavior was much smaller, maybe because direct ENSO-related diabatic heating effects were more important there. This assumption is consistent with the success of a simple persistence forecast, which was found over this region during ENSO. We also noticed that the persistence of the tropical convection was much weaker during warm ENSO years than during other years. This indicates that cool SSTs could effectively reduce convection but that warm SSTs did not immediately cause more convection. There exist strong qualitative similarities between this result and a recent paper from Tompkins (2001). In a comparable experimental design, he investigated the response of a cloud-resolving model to sudden changes of cold and warm SSTs. Even though this was a somewhat different model, he found a surprisingly similar result: Tropical convection died out quickly over cool SSTs, but convection did not spontaneously flare up over warm SSTs. Instead, convection propagated slowly toward the warm anomaly at a time scale of several weeks. Tompkins (2001) concluded that the slow advective adjustment time scale of water vapor is key to the memory of tropical dynamical circulations.

Despite the similarities between this study and previous work, and despite the good climatology of the model, we want to emphasize that this study was model based. Therefore, one must be careful when interpreting these results for the real atmosphere. In particular, it is important to note that the initial condition effect was closely related to convective activity and therefore to the kind of cumulus convection parameterization used. Since modern AGCMs are beginning to use the same scheme as our model (RAS), they are all likely to show similar features. Thus, independent of the question of real or artifact, this underlines the need for good tropical observations. Ultimately, this will not only improve tropical forecasts, but should also have positive impacts on extratropical long-range predictions.

Acknowledgments. We thank M. Kanamitsu for many insightful discussions and for his help with the model. The comments of three anonymous reviewers greatly helped to improve this paper. Funding for this research was provided by a cooperative agreement with NOAA (NA77RJ0435 and NA17R1231) and NASA Grant NAG8-175. The views expressed herein are those of the authors and do not reflect the views of NOAA and NASA. We thank the Maui High Performance Computing Center and the San Diego Supercomputing Center for providing computing time. This work is part of the Ph.D. thesis of T. Reichler.

APPENDIX

Forecast Skill

Before the forecast skill was calculated, the model data were treated in the following way: First, daily climatological means were computed at each grid point by averaging over R ensemble members and Y years of a specific experiment, that is,

$$\langle P(t, x)\rangle_{R,Y} = \frac{1}{RY}\sum_{r=1}^{R}\sum_{y=1}^{Y} P_{r,y}(t, x), \tag{A1}$$

where $P_{\gamma,y}(t,\ x)$ represents any predicted model variable for lead time t, location x, ensemble member r, and year y. Next, anomalies $P' = P - \langle P\rangle$ were calculated with respect to the daily climatology of each individual experiment. We refer to these anomalies as unfiltered data. Next, the anomalies were filtered in time by taking 31-day running means, that is,

$$\tilde{P}_{r,y}(t, x) = \frac{1}{2M+1}\sum_{l=-M}^{M} P'_{r,y}(t + l, x), \tag{A2}$$

with $M = 15$. This process is simply denoted as monthly averaging. The filtering was performed at each location, separately for the simulations of each individual member and year.

The forecast skill was estimated from correlations between a *prediction* and a *verification* experiment. In all cases, 10-member ensemble means of the experiment under consideration were used as prediction time series, that is,

$$\tilde{P}_y = \frac{1}{R}\sum_{r=1}^{R}\tilde{P}_{r,y}, \tag{A3}$$

and individual members of experiment ICBC were selected as a verification experiment.

Using daily model output, two forms of correlation measurements were used. First, we used the spatial anomaly correlation (AC) over the tropical sector, which was calculated as follows: Let $\tilde{P}_y$ be the prediction of any experiment, and $\tilde{V}_{r,y}$ be member r of the filtered verification field from ICBC; then

$$AC_{r,y}(t) = \frac{\displaystyle\int_X (\tilde{P}_y - \overline{P}_y)(\tilde{V}_{r,y} - \overline{V}_{r,y})\, dX}{\sqrt{\displaystyle\int_X (\tilde{P}_y - \overline{P}_y)^2\, dX \int_X (\tilde{V}_{r,y} - \overline{V}_{r,y})^2\, dX}} \tag{A4}$$

defines the spatial AC at lead time t, during year y, and using verification member r. Here, dX is the differential surface element of the tropical region X, and $\overline{P}$ and $\overline{V}$ are the respective area averages of $\tilde{P}$ and $\tilde{V}$, for example, $\overline{P} = 1/X \int_X \tilde{P}\, dX$. Since $R = 20$ members of experiment ICBC were available as verification members, the AC calculations were repeated for each individual member resulting in 20 different correlation estimates.

Averages of correlations were computed by first using a Fisher z transformation (e.g., Roads 1988) of the individual correlations, that is,

$$Z_{r,y} = \frac{1}{2}\ln\frac{(1 + AC_{r,y})}{(1 - AC_{r,y})}, \tag{A5}$$

and by then taking the arithmetic average, that is,

$$Z_y = \frac{1}{R}\sum_{r=1}^{R} Z_{r,y}. \tag{A6}$$

The final result was transformed back to regular correlations, that is,

$$AC_y = \frac{\exp(Z_y) - 1}{\exp(Z_y) + 1}. \tag{A7}$$

When experiment ICBC was verified against itself, again 10-member (instead of the possible 19 members) ensemble means were taken from ICBC as prediction, and another arbitrarily chosen member from ICBC was taken as the verification time series.

The second measure of forecast skill was the temporal correlation (TC) between the year-to-year time series of the verification experiment and the prediction experiment for the same lead time. The TCs are given by

$$TC_r(t, x) = \frac{\left\langle \left(\tilde{P}_y - \frac{1}{Y}\langle\tilde{P}_y\rangle\right)\left(\tilde{V}_{y,r} - \frac{1}{Y}\langle\tilde{V}_y\rangle\right)\right\rangle}{\sqrt{\left\langle\left(\tilde{P}_y - \frac{1}{Y}\langle\tilde{P}_y\rangle\right)^2\right\rangle\left\langle\left(\tilde{V}_{y,r} - \frac{1}{Y}\langle\tilde{V}_y\rangle\right)^2\right\rangle}}, \tag{A8}$$

where $\langle\cdots\rangle$ denotes a summation over the corresponding years. As for the ACs, the individual Fisher z–transformed TCs from using R verification members were averaged, and the final result was transformed back to regular correlations.

Variance ratios

The calculation of variance ratios was done in the following way: Seasonal mean anomalies were calculated for each year and member, that is,

$$\hat{P}_{r,y}(x) = \frac{1}{T - M}\sum_{t=M/2}^{T-M/2-1}\tilde{P}_{r,y}(x, t), \tag{A9}$$

where $T = 107$ is the length of each forecast time series in days, and $M = 15$. These seasonal mean anomalies were used to calculate the interannual variance of seasonal means, that is,

$$VIA(x) = \frac{1}{R * Y - 1}\left(\langle\hat{P}_{r,y}(x)^2\rangle - \frac{1}{R * Y}\langle\hat{P}_{r,y}(x)\rangle^2\right), \tag{A10}$$

where $\langle\cdots\rangle$ denotes a summation from $i = 0$ to $R * Y$. The intraseasonal variance was calculated from

$$VIS_{r,y}(x) = \frac{1}{T - M - 1}\left(\langle\tilde{P}_{r,y}(x)^2\rangle - \frac{1}{T - M}\langle\tilde{P}_{r,y}(x)\rangle^2\right), \tag{A11}$$

where $\langle\cdots\rangle$ denotes a summation over $t = M/2$ to $T - M/2 - 1$. The final VIS was taken from the average over all members and years.

REFERENCES

Anderson, J., H. Van den Dool, A. Barnston, W. Chen, W. Stern, and J. Ploshay, 1999: Present-day capabilities of numerical and statistical models for atmospheric extratropical seasonal simulation and prediction. *Bull. Amer. Meteor. Soc.,* **80,** 1349–1361.

Buizza, R., 1997: Potential forecast skill of ensemble prediction and spread and skill distributions of the ECMWF ensemble prediction system. *Mon. Wea. Rev.,* **125,** 99–119.

Goddard, L., and S. J. Mason, 2002: Sensitivity of seasonal climate forecasts to persisted SST anomalies. *Climate Dyn.,* **19,** 619–632.

Jin, F., and B. J. Hoskins, 1995: The direct response to tropical heating in a baroclinic atmosphere. *J. Atmos. Sci.,* **52,** 307–319.

Kalnay, E., and Coauthors, 1996: The NCEP/NCAR 40-Year Reanalysis Project. *Bull. Amer. Meteor. Soc.,* **77,** 437–471.

Kanamitsu, M., 1985: A study of the predictability of the ECMWF operational forecast model in the tropics. *J. Meteor. Soc. Japan,* **63,** 779–804.

——, W. Ebisuzaki, J. Woolen, S.-K. Yang, J. Hnilo, M. Fiorino, and G. L. Potter, 2002a: NCEP–DOE AMIP-II reanalysis (R-2). *Bull. Amer. Meteor. Soc.,* **83,** 1631–1643.

——, and Coauthors, 2002b: NCEP dynamical seasonal forecast system 2000. *Bull. Amer. Meteor. Soc.,* **83,** 1019–1037.

Kistler, R., and Coauthors, 2001: The NCEP–NCAR 50-year reanalysis: Monthly means CD-ROM and documentation. *Bull. Amer. Meteor. Soc.,* **82,** 247–267.

Madden, R. A., and P. R. Julian, 1994: Observations of the 40–50-day tropical oscillation—A review. *Mon. Wea. Rev.,* **122,** 814–837.

Mason, S. J., L. Goddard, N. E. Graham, E. Yulaeva, L. Q. Sun, and P. A. Arkin, 1999: The IRI seasonal climate prediction system and the 1997/98 El Niño event. *Bull. Amer. Meteor. Soc.,* **80,** 1853–1873.

Newell, R. E., and Z.-X. Wu, 1992: The interrelationship between temperature changes in the free atmosphere and sea-surface temperature changes. *J. Geophys. Res.,* **97D,** 3693–3709.

Reichler, T., and J. O. Roads, 2003: The role of boundary and initial conditions for dynamical seasonal predictability. *Nonlinear Processes Geophys.,* **10,** 211–232.

——, and ——, 2005: Long-range predictability in the Tropics. Part II: 30–60-day variability. *J. Climate,* **18,** 634–650.

Reynolds, C. A., P. J. Webster, and E. Kalnay, 1994: Random error growth in NMC global forecasts. *Mon. Wea. Rev.,* **122,** 1281–1305.

Reynolds, R. W., and T. M. Smith, 1994: Improved global sea surface temperature analyses using optimum interpolation. *J. Climate,* **7,** 929–948.

Roads, J. O., 1988: Lagged average predictions in a predictability experiment. *J. Atmos. Sci.,* **45,** 147–162.

——, S. C. Chen, and F. Fujioka, 2001: ECPC's weekly to seasonal global forecasts. *Bull. Amer. Meteor. Soc.,* **82,** 639–658.

Shukla, J., 1998: Predictability in the midst of chaos: A scientific basis for climate forecasting. *Science,* **282,** 728–731.

Tompkins, A. M., 2001: On the relationship between tropical convection and sea surface temperature. *J. Climate,* **14,** 633–637.

Toth, Z., and E. Kalnay, 1997: Ensemble forecasting at NCEP and the breeding method. *Mon. Wea. Rev.,* **125,** 3297–3319.

Xie, P. P., and P. A. Arkin, 1997: Global precipitation: A 17-year monthly analysis based on gauge observations, satellite estimates, and numerical model outputs. *Bull. Amer. Meteor. Soc.,* **78,** 2539–2558.

Yulaeva, E., and J. M. Wallace, 1994: The signature of ENSO in global temperature and precipitation fields derived from the microwave sounding unit. *J. Climate,* **7,** 1719–1736.